# Sub-Kelvin Stereodynamics of the Ne($^3P_2$) + N$_2$ Reaction

Junwen Zou, Sean D. S. Gordon, and Andreas Osterwalder[*]

*Institute for Chemical Sciences and Engineering, Ecole Polytechnique Fédérale de Lausanne (EPFL),
1015 Lausanne, Switzerland*

We present an experimental study of the low-energy stereodynamics of the Ne($^3P_2$) + N$_2$ reaction. Supersonic expansions of the two reactants are superposed in a merged beam experiment, where individual velocity control of the two beams allows us to reach average relative velocities of zero, yielding minimum collision energies around 60 mK. We combine the merged beam technique with the orientation of the metastable neon atoms and measure the branching between two reaction channels, Penning ionization and associative ionization, as a function of neon orientation and collision energy, covering the range 0.06–700 K. We find that we lose the ability to orient Ne below $\approx$100 K due to dynamic reorientation. Associative ionization products Ne-N$_2^+$ predissociate with a probability of 30%–60% and that associative ionization is entirely due to reactions of the $\Omega = 2$ state, where the singly occupied $p$ orbital of the Ne$^*$ is oriented along the interatomic axis.

*Introduction.*—Several groundbreaking studies have demonstrated the potential in recently developed experimental techniques to control and investigate chemical reactions at collision energies below 1 K [1–11]. One of these methods is the merged beam technique, which gives access to near-zero collision energies by superposing two supersonic expansions and reducing the relative velocity without the need for slow molecules in the laboratory reference frame. Different approaches for this have been proposed in the past, namely, the use of Stark decelerators and molecular synchrotrons [12], of backward-rotating nozzles [13], and of guides [14]. The first demonstrations of the merged beam approach were achieved by Henson *et al.* [4] and by Jankunas *et al.* [6], and it has since been applied to several studies that allowed for, e.g., the observation of shape resonances [4], symmetry-dependent reactivity [15], and stereodynamics [16].

In the realm of control, it is of special interest to actively fix also the reactant orientation [17–19]. Such stereodynamics experiments introduce an anisotropy and provide access to angular dependencies that are not accessible when using isotropically distributed reactants [20,21]. The combination of low-energy collisions with steric control is interesting particularly in view of effects like dynamic reorientation, which can take place at low collision energies, when the force from the interatomic potential overcomes the force produced by the external magnetic field. Thus, at the lowest energies, the stereodynamics are entirely dominated by the potential between the reactants rather than by kinematics or external fields, thus completely changing the outcome of the reaction. The energy at which the ability to orient is lost, as observed recently for several prototypical reactions [16,22], depends on the interaction potential between the two reactants. Here we here apply the merged beam technique to the investigation of the reorientation effect in detail.

In collisions between an excited atom $A^*$ and a ground state particle $BC$ with an ionization energy lower than the internal energy of reactant $A^*$, three primary reactions can take place,

$$A^* + BC \rightarrow A + BC^+ + e^-, \tag{1}$$

$$\rightarrow ABC^+ + e^-, \quad \text{and} \tag{2}$$

$$\rightarrow A + B + C^+ + e^-, \tag{3}$$
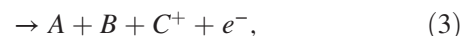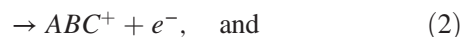
called Penning ionization (PI), associative ionization (AI), and dissociative ionization, respectively [23,24]. They have all been studied extensively in the past decades, both theoretically and experimentally [25–28].

We have found in the past that the atoms that emerge from our magnetic guide are polarized and can be oriented even by very weak stray fields [29], and our Ne($^3P_2$) + Ar studies demonstrate that it is critical to know the exact state of the Ne($^3P_2$) atoms when measuring branching ratios. With unknown orientation or polarization, reactivity measurements become very difficult to interpret, and care must be taken to apply appropriate models [30]. In a recent study of the Ne($^3P_2$) + Ar reaction, we have measured the branching between reactions (1) and (2) in the energy range 0.02–1000 K, while controlling the orientation of the Ne($^3P_2$) atoms (henceforth, Ne$^*$) with an external magnetic field [16]. This effectively controls the populations of states with different $\vec{J}$ projections on the interatomic axis. Ne$^*$

itself has an anisotropic electron distribution, making also the propensities for AI and PI angle dependent. A strong steric effect was observed, except at the lowest collision energies where the branching ratio was independent of the external magnetic field, an effect we attributed to a reorientation of $Ne^*$.

Here we extend our studies to the investigation of the (oriented $Ne^*$) + $N_2$ reaction and present sub-Kelvin stereodynamics studies of a triatomic collision system. In contrast to atom + atom reactions, atom + molecule reactions possess more internal structure and offer a higher complexity even if the molecule itself is not oriented. In the case of $N_2$, for example, the existence of a vibrational structure has been observed to significantly affect the branching ratio [31,32]. We recently found that predissociation can distort the measured channel branching: products of reaction 2 usually are weakly bound $Ne-N_2^+$ complexes, where the $N_2$ fragment can be formed in excited states. Energy flow from the $N_2$ fragment to the $Ne-N_2^+$ bond can then lead to predissociation. PI can thus lead to the same product ions as AI followed by predissociation, namely, bare $N_2^+$, while AI alone should form $Ne-N_2^+$ complex cations [32]. Expanding our high-energy studies to less than 0.1 K allows us to compare them with those from Ref. [16] to extract separate propensities for AI and PI and to improve our understanding of the energy-dependent reaction mechanisms.

*Experimental details.*—A detailed description of the complete setup is given elsewhere [5,33]. Briefly, a supersonic expansion of state-purified metastable $Ne(^3P_2)$ is merged with a supersonic expansion of $N_2$ by bending the neon onto the axis of the $N_2$, using a 1.8 m long, curved permanent-magnet multipole guide. The guiding dynamics inside the guide depend on the magnetic quantum number that leads to a polarized $Ne^*$. The $Ne^*$ speed is controlled by varying the valve temperature from $\approx$ 200–250 K, yielding center velocities between 700 and 760 m/s. $N_2$ is formed by expanding a mixture of He and $N_2$, and injected tangentially through the magnetic guide. Velocities of 750–1700 m/s are obtained by varying the He:$N_2$ seeding ratio between 1:10 and 30:1, which leads, in combination with the $Ne^*$ velocities, to collision energies in the range from $E_{coll}/k_B = 60$ mK to 700 K ($k_B$ is the Boltzmann constant). From our previous measurements, we estimate the rotational temperature of $N_2$ in the molecular beam to be $\sim 20$ K, which implies that more than 97% of molecules occupy levels with $J \leq 4$ [32].

The two beams enter an area with a controlled magnetic field that is produced through two pairs of solenoid magnets arranged at 90 deg (see Fig. 1), which allows the production of a magnetic field with a well-defined direction at any angle [32]. Polarized $Ne^*$ atoms emerge from the magnetic guide and are adiabatically oriented in the magnetic field. Reaction products, either $N_2^+$ or $Ne-N_2^+$, are extracted in a pulsed time-of-flight mass spectrometer out of the plane of Fig. 1.
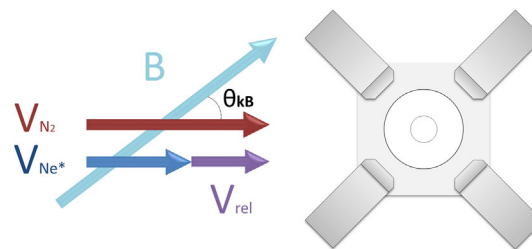


FIG. 1. Sketch of the interaction region. Two parallel molecular beams collide with the relative velocity $v_{rel}$ in the center of a pair of solenoids, arranged at 90 deg, which produces the magnetic field $\vec{B}$ at an angle $\theta_{kB}$.

The populations for the different $m_J$ states have been determined spectroscopically [29,33]. It should be noted that the measured populations are not what one would expect based on trajectory calculations alone since it appears that some degree of depolarization is taking place between the end of the magnetic guide and the interaction zone 30 cm away; a scattering experiment comparing different reactions of magnetically or electrically controlled particles must include a detailed analysis of the polarization.

The populations, together with the selected angle $\theta_{kB}$ between $\vec{B}$ and $\vec{k}$, are used to calculate populations in the molecular reference frame where the projection of $\vec{J}$ on the interparticle axis is labeled by $\Omega$, in analogy with Hund's coupling case (c). Wigner $D$ matrices are used, for each magnetic field orientation, to determine the $p(\Omega)$ populations from the measured $p(m_J)$. Previous experiments indicate that AI products are formed with several quanta of vibrational excitation of the $N_2^+$ bound to Ne [31,32], and all but the ground state products predissociate, presumably in most cases on a very fast timescale [34].

Examples of raw data traces are shown in Fig. 2. Figures 2(a) and 2(b) show mass spectra recorded at an angle of $\theta_{kB} = 85°$ and at collision energies of $E_{coll}/k_B = 68$ mK and 616 K, respectively. $N_2^+$ (the early, red-shaded
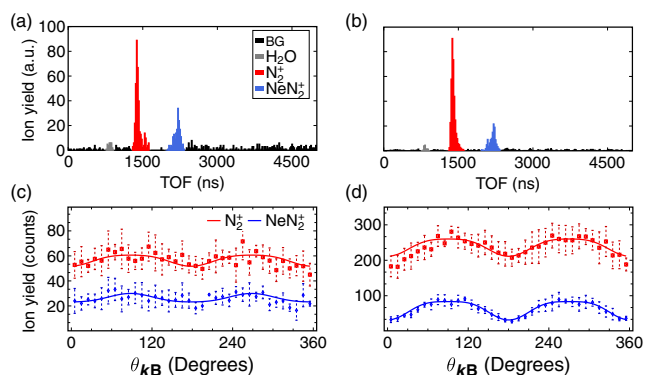


FIG. 2. Samples of raw TOF spectra at $\theta_{kB} = 85°$ for (a) $E_{coll}/k_B = 68$ mK and (b) $E_{coll}/k_B = 616$ K. (c),(d) Ion yields as a function of $\theta_{kB}$ for the same collision energies. BG is short for background.

signal) and $NeN_2^+$ (late, blue) are easily distinguished. Figures 2(c) and 2(d) show the angle-dependent total ion counts for the two energies, and in each case the red (blue) trace corresponds to the $N_2^+$ ($NeN_2^+$) signal. These signals contain information on the $\Omega$ specific reaction cross sections for AI and PI, as well as for the propensity for predissociation of the $NeN_2^+$ products. Our studies of $Ne^* + Rg$ have shown that the AI channel is enhanced when the singly occupied $p$ orbital on $Ne^*$ is oriented along the interatomic axis (corresponding to $\Omega = 2$), while PI takes place at longer internuclear distances and has an angle-independent propensity, and this was the case for $Rg = Ar$, Xe, and Kr [32]. We can use that result to disentangle the true AI and PI signals from the measured ion signals: we assume that the measured $N_2^+$ signal carries an angle-independent part (PI) and an angle-dependent part that originates from predissociated AI products, and we write

$$I_{N_2^+}(\theta_{kB}, E_{coll}) = w(E_{coll}) I_{NeN_2^+}(\theta_{kB}, E_{coll}) + I_{PI}(E_{coll}), \quad (4)$$

where $\theta_{kB}$ is the angle between relative velocity $\vec{k}$ and magnetic field direction $\vec{B}$, $E_{coll}$ is the collision energy, $w(E_{coll})$ is the fraction of $NeN_2^+$ ions that predissociate, and $I_{PI}(E_{coll})$ is the fraction of $N_2^+$ ions that are formed through direct PI. $w(E_{coll})$ and $I_{PI}(E_{coll})$ do not depend on the magnetic field direction, but they can vary with collision energy. The predissociation probability of the AI products can then be written as $P_{pd}(E_{coll}) = [w(E_{coll})/1 + w(E_{coll})]$. The actual ratio between AI and PI thus becomes

$$R(\theta_{kB}) = \frac{I_{AI}}{I_{PI}} = \frac{I_{NeN_2^+}(\theta_{kB}) + wI_{NeN_2^+}(\theta_{kB})}{I_{N_2^+}(\theta_{kB}) - wI_{NeN_2^+}(\theta_{kB})}, \quad (5)$$

which defines the reactivity $R$. As we show below, this approximation is justified only at collision energies above $\approx 30$ K where we observe a steric effect. Below that, the reactivity becomes independent of $\theta_{kB}$, and we write it directly as the ratio between the ion signals $R_{low\_E}(\theta_{kB}) = [I_{NeN_2^+}(\theta_{kB})/I_{N_2^+}(\theta_{kB})]$.

*Results and discussion.*—To extract relative reaction cross sections for AI and PI, we express each of the channels as $I_{AI,PI} \propto \sum_{\Omega=0,1,2} p(\Omega)\sigma^{AI,PI}$ and fit the measured ratio $R$ to the ratio $I_{AI}/I_{PI}$ [33]. The primary results from this analysis are the $\Omega$ specific ratios $\sigma_{AI}^{\Omega}/\sigma_{PI}^{\Omega}$. Figures 3(a) and 3(b) show the raw and fitted reactivity, respectively, as a function of orientation angle and collision energy. The reactivity on the right side, above 30 K, is obtained using Eq. (5), while the one on the left is the ratio of the raw ion signals. Above 30 K, the ratio between AI and PI strongly depends on $\theta_{kB}$, while it is nearly independent of collision energy. As the orientation angle $\theta_{kB}$ is varied from $0°$ to $360°$, the reaction oscillates
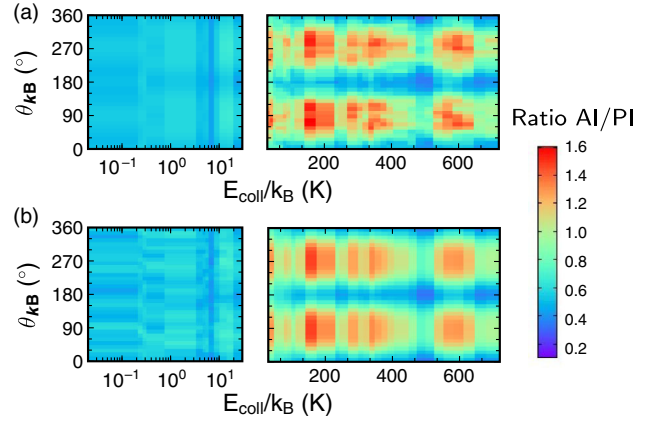


FIG. 3. Experimental (a) and fitted (b) reactivity as a function of collision angle and energy. In both cases, the left side shows the energy range 0.06–30 K, and the right side shows the range 30–700 K. (Left) Raw data. (Right) The true AI/PI obtained through a fit of Eq. (4).

between PI dominated and AI dominated. This is in stark contrast with the $Ne^* + Ar$ reaction where, despite the angle-dependent oscillations, PI dominates at low collision energies but is the minor channel at high energies.

$\Omega$ specific reactivities are shown in Figs. 4(a)–4(c) for $\Omega = 0$, 1, and 2, respectively. In each case, the left panel for $E_{coll} < 30$ K is obtained from $R_{low\_E}$, while the right panel uses Eq. (5) and excludes predissociation. Three striking observations can be made here: (1) While the $\Omega = 0$, 1 reactivities are nearly zero at high energies and rise to $\approx 0.5$ below 30 K, the $\Omega = 2$ reactivity is around 2.5 at high energies and steeply drops to $\approx 0.6$ below 30 K. (2) AI above 30 K originates exclusively from the $\Omega = 2$ state. The AI channel is closed for $\Omega = 0$, 1. (3) Below 30 K, the efficiency of the AI channel is lower than that of the PI channel for all $\Omega$ values. Further information is obtained by calculating the energy-dependent ratio $R(90°)/R(180°)$, being the ratio between the maximum and minimum of curves like those in Figs. 2(c) and 2(d). This ratio, shown in Fig. 4(d), quantifies the steric effect; it is close to 1 if there is no angle dependence. Similar to our observation in $Ne^* + Ar$ collisions, the steric effect is quite pronounced at energies above 100 K but then drops and is absent below 10 K. At the lowest collision energies (indicated by a pink shading), our experiment does not permit orientational control since in this range the longitudinal relative velocities become comparable to the spread of the transverse velocities.

Finally, Fig. 5 shows $P_{pd}$, the probability for predissociation of AI products as a function of energy, as extracted through a least-squares fit of Eq. (4) to the raw data. As the collision energy decreases, a slight downward trend is observed for $w$, which implies that the state distribution of the $Ne-N_2^+$ ions changes as a function of collision energy. Sonnenfroh and Leone have studied this reaction in the past and found the vibrational state
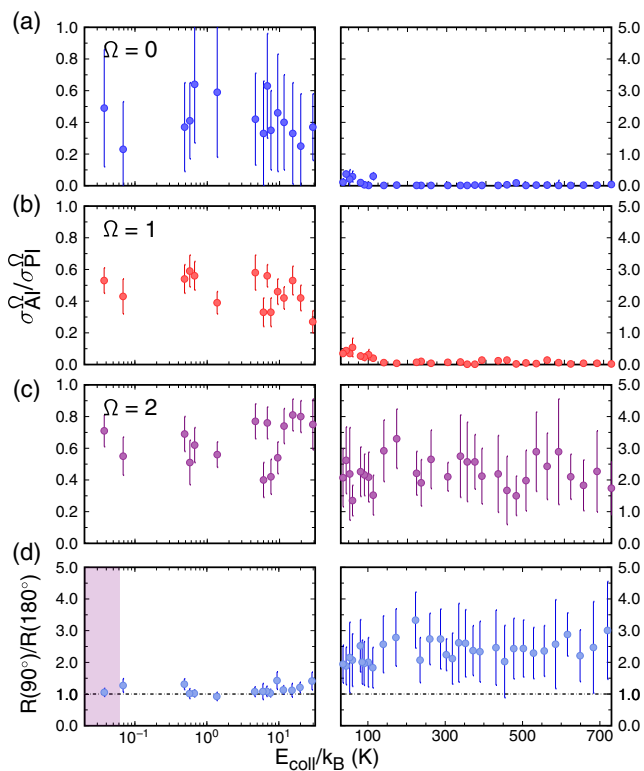
FIG. 4. Reaction cross section ratios for $\Omega = 0$, 1, and 2 (a)–(c). Error bars are one standard deviation of the cross section histograms as obtained from the fit. (d) The steric effect as a function of energy. The pink-shaded area shows the range where transverse and longitudinal velocities are comparable. (Left) Results are from fits to the raw reactivity $R_{\text{low\_}E}$. (Right) The corrected reactivity $R$ was used.



FIG. 5. The probability $P_{\text{pd}}$ for predissociation of the AI products Ne-$N_2^+$, obtained by fitting Eq. (4) to the experimental data.

distributions to be largely governed by Franck-Condon factors [31]. Possibly, the changing wave function of the collision complex leads to sufficiently strong variations of those, even though we here only cover an energy range of 0.1 eV relative to the energy release of more than 1 eV during ionization. Recent calculations propose the existence of long-lived states where predissociation is suppressed, and the collision-energy-dependent population of such states would have a great effect on the observed predissociation rate [35].

A particularly intriguing feature in Fig. 5 is the local reduction of $P_{\text{pd}}$ observed around 470 K, a collision energy where we also observe a reduced propensity for AI, see Fig. 3. This energy coincides with the calculated energy of the $v^+ = 4$ state of $N_2^+$, using $\omega_e = 2207$ cm$^{-1}$ and $\omega_e x_e = 16$ cm$^{-1}$, in combination with the energies of Ne* (16.6 eV) and the ionization potential of $N_2$ (15.58 eV) and the estimated binding energy of Ne to $N_2$ of 300 cm$^{-1}$ [31,36]. We tentatively assign the feature to a vibrational Feshbach resonance that leads to the formation of Ne-$N_2^+$ with $N_2^+$ in the vibrationally excited state. A final assignment requires additional experiments that enable us to
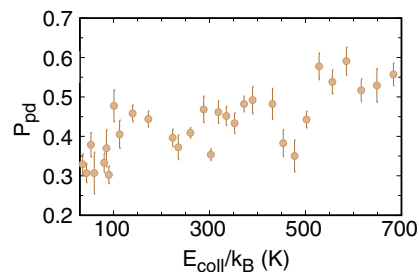
separately detect the formation of this complex prior to predissociation, as well as theoretical calculations.

The electronic configuration of Ne* is $1s^2 2s^2 2p^5 3s^1$. A magnetic quantum number $m_J = 2$ implies that the singly occupied $2p$ orbital is oriented along the selected axis, which in turn means that in the $\Omega = 2$ state it is oriented along the interparticle axis. Similar to our previous study on the Ne* + Ar reaction [16,32], we find that AI necessitates $\Omega = 2$. In other words, the orbital overlap that is required for complex formation preceding AI is very strongly favored by that particular Ne* orientation. In contrast to the case of Ar, however, we here observe no AI from $\Omega = 0$, 1 at all. Only when the collision energy is reduced below a certain threshold do we observe AI from all three components. However, this only happens when the Ne* electron distribution dynamically reorients into the most stable arrangement relative to $N_2$, which corresponds an arrangement similar to the $\Omega = 2$ state, since in this configuration a metastably bound Ne*-$N_2$ complex can be formed. The energy range in which we start observing this reorientation is very similar for Ar and $N_2$, which can be explained by the similar interaction potentials between Ne* and either of these species [37].

*Conclusions.*—The stereodynamics of the Ne* + $N_2$ reaction shows several similarities to the Ne* + Ar reaction: in both cases associative ionization originates predominantly from Ne($^3P_2$, $\Omega = 2$) states, while the other components show little (in the case of Ar) or no associative ionization. In both reactions, the steric control is lost to dynamic reorientation at around 30 K, a similarity that is expected from the comparable interaction potentials of Ne* with the two reactants. Although the Ne* + $N_2$ interaction potential is anisotropic, there is no signature of this in the present data because the nonzero rotational temperature of $N_2$ leaves some population in rotationally excited states and effectively turns the molecule into an isotropic object. The added complexity of $N_2$ in comparison with Ar is seen primarily in the additional dynamics of the product ion, namely, that an AI product can predissociate. We find the total probability for predissociation to be 30%–60% over the entire energy range covered here, but to slightly increase with collision energy. Below 30 K, our experiment

does not currently allow us to extract information on the predissociation.

The very strong dependence of the AI/PI ratio on the $p(\Omega)$ implies that great care must be taken when interpreting experimental results. Any kind of manipulation of polar or paramagnetic particles with electric or magnetic fields induces some degree of polarization. Depolarization dynamics eliminate the effect of the fields once the particles emerge from them, but depending on the system the relevant timescales may well be on the timescale of the experiment. Depending on the subsequent experiment, it is critical to quantify the polarization in view of a correct analysis of reaction cross sections and branching ratios.

---

[*]andreas.osterwalder@epfl.ch

[1] R. V. Krems, B. Friedrich, and W. C. Stwalley, *Cold Molecules: Theory, Experiment, Applications* (CRC Press, Boca Raton, FL, 2009).

[2] *Cold Chemistry: Molecular Scattering and Reactivity near Absolute Zero*, edited by O. Dulieu and A. Osterwalder (Royal Society of Chemistry, Cambridge, England, 2017).

[3] S. Y. T. van de Meerakker, H. L. Bethlem, N. Vanhaecke, and G. Meijer, Chem. Rev. **112,** 4828 (2012).

[4] A. B. Henson, S. Gersten, Y. Shagam, J. Narevicius, and E. Narevicius, Science **338,** 234 (2012).

[5] A. Osterwalder, EPJ Tech. Instrum. **2,** 10 (2015).

[6] J. Jankunas, B. Bertsche, K. Jachymski, M. Hapka, and A. Osterwalder, J. Chem. Phys. **140,** 244302 (2014).

[7] S. Chefdeville, T. Stoecklin, A. Bergeat, K. M. Hickson, C. Naulin, and M. Costes, Phys. Rev. Lett. **109,** 023201 (2012).

[8] S. N. Vogels, J. Onvlee, S. Chefdeville, A. van der Avoird, G. C. Groenenboom, and S. Y. van de Meerakker, Science **350,** 787 (2015).

[9] W. E. Perreault, N. Mukherjee, and R. N. Zare, Science **358,** 356 (2017).

[10] C. Amarasinghe and A. G. Suits, J. Phys. Chem. Lett. **8,** 5153 (2017).

[11] A. P. P. van der Poel, P. C. Zieger, S. Y. T. van de Meerakker, J. Loreau, A. van der Avoird, and H. L. Bethlem, Phys. Rev. Lett. **120,** 033402 (2018).

[12] S. Y. T. van de Meerakker and G. Meijer, Faraday Discuss. **142,** 113 (2009).

[13] Q. Wei, I. Lyuksyutov, and D. R. Herschbach, J. Chem. Phys. **137,** 054202 (2012).

[14] G. Di Domenicantonio, B. Bertsche, and A. Osterwalder, Chimia **65,** 725 (2011).

[15] Y. Shagam, A. Klein, W. Skomorowski, R. Yun, V. Averbukh, C. P. Koch, and E. Narevicius, Nat. Chem. **7,** 921 (2015).

[16] S. D. S. Gordon, J. J. Omiste, J. Zou, S. Tanteri, P. Brumer, and A. Osterwalder, Nat. Chem. **10,** 1190 (2018).

[17] A. J. Orr-Ewing and R. N. Zare, Annu. Rev. Phys. Chem. **45,** 315 (1994).

[18] D. Watanabe, H. Ohoyama, T. Matsumura, and T. Kasai, Phys. Rev. Lett. **99,** 043201 (2007).

[19] H. Ohoyama, K. Yasuda, and T. Kasai, J. Phys. Chem. A **112,** 10716 (2008).

[20] M. Brouard and C. Vallance, *Tutorials in Molecular Reaction Dynamics* (Royal Society of Chemistry, Cambridge, England, 2011).

[21] F. Aoiz, M. Brouard, S. Gordon, B. Nichols, S. Stolte, and V. Walpole, Phys. Chem. Chem. Phys. **17,** 30210 (2015).

[22] W. E. Perreault, N. Mukherjee, and R. N. Zare, Nat. Chem. **10,** 561 (2018).

[23] J. Jankunas, B. Bertsche, and A. Osterwalder, J. Phys. Chem. A **118,** 3875 (2014).

[24] B. Brunetti, S. Falcinelli, A. Sassara, J. de Andres, and F. Vecchiocattivi, Chem. Phys. **209,** 205 (1996).

[25] W. H. Miller, J. Chem. Phys. **52,** 3563 (1970).

[26] P. Siska, Rev. Mod. Phys. **65,** 337 (1993).

[27] H. Hotop, J. Lorenzen, and A. Zastrow, J. Electron Spectrosc. Relat. Phenom. **23,** 347 (1981).

[28] S. Falcinelli, A. Bartocci, S. Cavalli, F. Pirani, and F. Vecchiocattivi, J. Chem. Phys. **143,** 164306 (2015).

[29] J. Jankunas, K. S. Reisyan, T. P. Rakitzis, and A. Osterwalder, Mol. Phys. **114,** 245 (2016).

[30] N. Bibelnik, S. Gersten, A. B. Henson, E. Lavert-Ofir, Y. Shagam, W. Skomorowski, C. P. Koch, and E. Narevicius, Mol. Phys. **117,** 2128 (2019).

[31] D. M. Sonnenfroh and S. R. Leone, Int. J. Mass Spectrom. **80,** 63 (1987).

[32] J. Zou, S. D. S. Gordon, S. Tanteri, and A. Osterwalder, J. Chem. Phys. **148,** 164310 (2018).

[33] S. D. S. Gordon, J. Zou, S. Tanteri, J. Jankunas, and A. Osterwalder, Phys. Rev. Lett. **119,** 053001 (2017).

[34] E. Bieske, A. Soliva, and J. Maier, J. Chem. Phys. **94,** 4749 (1991).

[35] A. Blech, Y. Shagam, N. Hölsch, P. Paliwal, W. Skomorowski, J. W. Rosenberg, N. Bibelnik, O. Heber, D. M. Reich, E. Narevicius *et al.*, arXiv:1902.09262.

[36] NIST Chemistry Webbook, https://webbook.nist.gov/chemistry/.

[37] J. Baudon, P. Feron, C. Miniatura, F. Perales, J. Reinhardt, J. Robert, H. Haberland, B. Brunetti, and F. Vecchiocattivi, J. Chem. Phys. **95,** 1801 (1991).